Antiferro- and metamagnetism in the $S = 7/2$ hollandite analog $EuGa_2Sb_2$

Tanya Berry [1,2,*] Sean R. Parkin [3] and Tyrel M. McQueen [1,2,4,†]

[1]*Department of Chemistry, The Johns Hopkins University, Baltimore, Maryland 21218, USA*

[2]*Institute for Quantum Matter, Department of Physics and Astronomy, The Johns Hopkins University, Baltimore, Maryland 21218, USA*

[3]*Department of Chemistry, University of Kentucky, Lexington, Kentucky 40506, USA*

[4]*Department of Materials Science and Engineering, The Johns Hopkins University, Baltimore, Maryland 21218, USA*

(Received 12 August 2021; accepted 6 October 2021; published 5 November 2021)

Recent work analyzing the impact of nonsymmorphic symmetries on electronic states has given rise to the discovery of multiple types of topological matter. Here we report the single-crystal synthesis and magnetic properties of $EuGa_2Sb_2$, a Eu-based antiferromagnet structurally consisting of pseudo-1D chains of Eu ions related by a nonsymmorphic glide plane. We find the onset of antiferromagnetic order at $T_N = 8$ K. Above T_N the magnetic susceptibility is isotropic. Curie-Weiss analysis suggests competing ferromagnetic and antiferromagnetic interactions, with $p_{\text{eff}} = 8.1\,\mu_B$ as expected for $4f^7$ $J = S = 7/2$ Eu^{2+} ions. Below T_N and at low applied magnetic fields, an anisotropy develops linearly, reaching $\chi_\perp/\chi_\parallel = 6$ at $T = 2$ K. There is concomitant metamagnetic behavior along $\chi_\parallel$, with a magnetic field of $\mu_0 H \approx 0.5$ T sufficient to suppress the anisotropy. Independent of crystal orientation, there is a continuous evolution to a field-polarized paramagnetic state with $M = 7\mu_B/Eu^{2+}$ at $\mu_0 H = 2$ T as $T \to 0$ K. Specific-heat measurements show a recovered magnetic entropy of $\Delta S_{\text{mag}} \approx 16.4\,\text{J mol}^{-1}\,\text{K}^{-1}$ from $T{\sim}0$ K to $T = T_N$, close to the expected value of $R\ln(8)$ for an $S = 7/2$ ion, indicating negligible low-dimensional spin fluctuations above T_N. We find no evidence of unusual behaviors arising either from the dimensionality or the presence of the nonsymmorphic symmetries.

DOI: 10.1103/PhysRevMaterials.5.114401

I. INTRODUCTION

Zintl phase compounds have earned a great deal of recognition due to their polyanionic and cationic networks in areas of thermoelectric, topological materials, and magnetic materials [1–10]. The structural motifs offered by Zintl phase materials are quite appealing due to the electrostatic interactions between cations and anions and covalent interactions in the polyanionic framework. This setting causes the materials to often behave as two independent subunits, with separate magnetic and electronic behaviors from the cations and polyanionic framework if the cations are magnetic and the anions are nonmagnetic.

When the cation is magnetic, the interplay between magnetism and structure could yield versatile ground states. Rare-earth based Zintl materials is extensively studied in terms of electronic transport. However, their magnetic structures have scarcely been studied [11–15].

Similarly, recent work has demonstrated how nonsymmorphic symmetries can conspire to generate unique topological electronic states of matter, such as Dirac sixfold and eightfold fermions, as well as more general topological states such as those found in $GdSb_xTe_{2-x-\delta}$, CeSbTe, and GdSbTe [16–22].

The magnetic Zintl phase $EuGa_2Sb_2$ was recently reported to exist based on a polycrystalline synthesis [23]. The reported crystal structure from single-crystal x-ray diffraction [24,25] has space group *Pnma* and has nonsymmorphic symmetries that relate to adjacent magnetic ions. Further, electron counting implies divalent Eu^{2+}, which has a half-filled f shell ($4f^7$) and $L = 0$, which considerably simplifies the interpretation of magnetic behavior [24,25]. Thus, $EuGa_2Sb_2$ provides an opportunity to explore the effects of nonsymmorphic symmetries on magnetic order.

This work reports the synthesis of single crystals of $EuGa_2Sb_2$ via flux growth, confirms the crystal structure by single-crystal x-ray diffraction, and studies the magnetic properties via magnetization and specific-heat measurements. The crystal structure is describable as an analog of Hollandite, with a Ga_2Sb_2 framework forming 1D channels in which Eu ions form pseudo-1D chains. We find the onset of antiferromagnetic order at $T_N = 8$ K, consistent with Mössbauer experiments [24]. Above T_N, Curie-Weiss analysis yields $p_{\text{eff}} = 8.1\,\mu_B$ as expected for $4f^7$ $J = S = 7/2$ Eu^{2+} ions. A positive Weiss temperature $\theta = 5.89$ K suggests competing ferromagnetic and antiferromagnetic interactions. The magnetic susceptibility is direction independent above T_N, with an anisotropy developing linearly below T_N, reaching $\chi_\perp/\chi_\parallel = 6$ at $T = 2$ K. There is concomitant metamagnetic behavior along $\chi_\parallel$, with a magnetic field of $\mu_0 H \approx 0.5$ T sufficient to suppress the anisotropy. There is also a continuous evolution to a field-polarized paramagnetic state with $M = 7\mu_B/Eu^{2+}$ at $\mu_0 H = 2$ T as $T \to 0$ K. Specific-heat measurements show a sharp transition at T_N, with a broad tail of entropy loss at lower temperatures. The estimated recovered magnetic entropy of $\Delta S_{\text{mag}} = 16.4\,\text{J mol}^{-1}\,\text{K}^{-1}$ from $T{\sim}0$ K to $T = T_N$ is close to the expected value of $R\ln(8)$ for an $S = 7/2$ ion. This behavior indicates little low-dimensional spin fluctuations above T_N, despite the low dimensionality implied by the crystal

*tberry9@jhu.edu
†mcqueen@jhu.edu

structure, and attributed to the large value of S. Together, these results allow us to gain insights into the nature of magnetism in Eu-based Zintl compounds and its correlation to the structure and thermodynamics quantities.

II. METHODS

A. Experiment

Single crystals of $EuGa_2Sb_2$ were synthesized from Eu (ingot, Yeemeida Technology Co., LTD 99.995%), Ga (ingot, Noah Tech 99.99%), and Sb (BTC, 99.999%) using the binary flux technique. The elements were put in Canfield crucibles (size: 2 mL) in 50:110:150 ratio for Eu:Ga:Sb with a total composition mass of 5 g. Ga and Sb were placed in the crucible at atmospheric conditions, while Eu was added last in an Ar-filled glove box. The Canfield crucible was placed in a quartz ampoule with quartz wool below and above the crucible, evacuated, and sealed under 1.2×10^{-2} Torr of pressure [26]. The evacuated ampoules were loaded in a box furnace at an angle of 45°. The temperature was ramped at 80 °C/h to $T = 550$ °C for 12 h. This step allows for Ga and Sb binary flux to be in a liquid state. The furnace was then ramped from $T = 550$ °C to $T = 1100$ °C at the rate of 80 °C/h and held for 24 h. The furnace was then slowly cooled to $T = 650$ °C at the rate of 5 °C/h, then removed hot, inverted, and immediately centrifuged. Centrifugation took 2–3 min. Rod-shaped crystals of size 1–1.5 mm along the long direction were removed from the frit. These single crystals of $EuGa_2Sb_2$ were found to be stable on the benchtop.

Powder x-ray diffraction (XRD) patterns were collected over an angle range of 5°–60° on a laboratory Bruker D8 Focus diffractometer that utilizes a LynxEye detector and Cu Kα radiation. Structural refinements were performed with GSAS-II, and resulting structures were visualized with VESTA software [27]. Single-crystal x-ray data were collected on a Bruker-Nonius X8 Proteum (Mo Kα radiation) diffractometer. SADABS was used to apply the absorption correction using the "multiscan" approach [27]. All calculations were performed using the SHELX software package. The structures were solved by direct methods, and successive interpretations of difference Fourier maps were followed by least-squares refinement [28,29].

Magnetization data were collected on a Quantum Design Magnetic Property Measurement System (MPMS). Magnetic susceptibility was approximated as magnetization divided by the applied magnetic field ($\chi \approx M/H$). In addition, heat capacity data were collected on a Quantum Design Physical Properties Measurement System using the semiadiabatic method and a 1% temperature rise.

TABLE I. Single crystal x-ray diffraction (SXRD) parameters and refinement statistics.

Formula	$EuGa_2Sb_2$
Crystal system	Orthorhombic
Space group	*Pnma* (No. 62)
a (Å)	18.2201(4)
b (Å)	4.2987(1)
c (Å)	6.6994(1)
V (Å^3)	524.715(19)
Z	4
M/gmol^{-1}	534.93
ρ_0/g cm^{-3}	6.772
μ/mm^{-1}	31.895
Radiation	Mo Kα, $\lambda = 0.710\,73$ Å
Temperature (K)	90 K
Reflections collected/number of parameters	1481/86
Goodness of fit	1.373
$R[F]$[a]	0.0207
$R_w(F_o^2)$[b]	0.005 10

[a] $R(\boldsymbol{F}) = \Sigma||\boldsymbol{F_o}| - |\boldsymbol{F_c}||/\Sigma|\boldsymbol{F_o}|$.
[b] $R_w(\boldsymbol{F_o^2}) = [\Sigma w(\boldsymbol{F_o^2} - \boldsymbol{F_c^2})^2/\Sigma w(\boldsymbol{F_o^2})^2]^{1/2}$.

III. RESULTS AND DISCUSSION

A. Structure

Powder XRD scans of $EuGa_2Sb_2$ were consistent with the previously reported structure in space group *Pnma* (62).

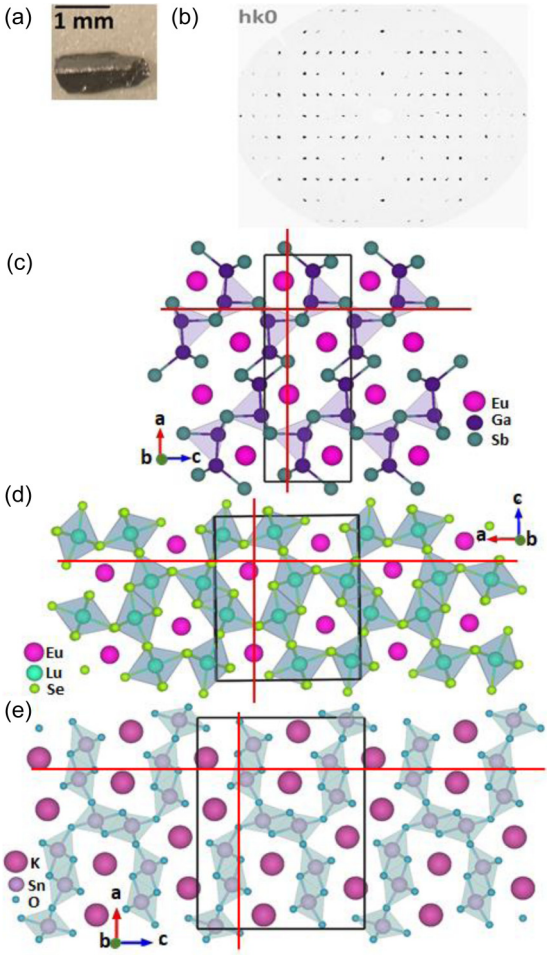

FIG. 1. (a) As-grown single-crystal image of $EuGa_2Sb_2$. (b) Single-crystal precision image of ($hk0$) plane. Structures of (c) $EuGa_2Sb_2$ [23–25], (d) $EuLu_2Se_4$ [30], and (e) $K_2Sn_3O_7$ [31] that crystallize in *Pnma* and are Hollandite-like structures containing 1D chains of ions in channels; red lines indicate the nonsymmorphic glide planes. The black box represents a unit-cell single-crystal x-ray diffraction.

TABLE II. Atomic coordinates for EuGa2Sb2 determined by SXRD.

	Occ.	Wyckoff positions	x (Å)	y (Å)	z (Å)	U_{eq}(Å^2)
Eu	1	4c	0.3847(1)	0.7500	0.7802(1)	0.003(1)
Ga1	1	4c	0.4293(1)	0.2500	0.4418(1)	0.004(1)
Ga2	1	4c	0.2921(1)	0.2500	0.4636(1)	0.004(1)
Sb1	1	4c	0.2872(1)	0.2500	0.0640(1)	0.003(1)
Sb2	1	4c	0.4694(1)	−0.2500	0.2315(1)	0.003(1)

The as-grown single crystals of $EuGa_2Sb_2$ showed phase purity via powder refinement. The results of single-crystal diffraction data refinements, Tables I, II, and III, are consistent with the prior literature reports from powder diffraction refinements. The as-grown single crystal is shown in Fig. 1(a) and a precision image from single-crystal refinement image is shown in Fig. 1(b). From an electron-counting perspective, the compound is expected to be built of Eu^{2+} cations, and a $[Ga_2Sb_2]^{2-}$ anionic Zintl framework, and that is indeed the case. Figure 1(c) shows that the structure is built of $[Ga_2Sb_2]^{2-}$ units that form structural motifs of tetrahedral and bridging Sb in a square-chain ladder format [23–25]. The squares consist of two bridging Sb and two Ga atoms, and the ladder consist of Ga-Ga chains. These form an extended network with one-dimensional channels in which Eu^{2+} ions reside.

The $EuGa_2Sb_2$ structure is comparable to $EuLu_2Se_4$ and $K_2Sn_3O_7$, crystallizing in the *Pnma* space group and analogous to the Hollandite structure type [30,31]. In Figs. 1(d) and 1(e), we see the classic $\alpha-MnO_2$ structure type of Hollandite in $EuLu_2Se_4$ and $K_2Sn_3O_7$. In these structures, there is a presence of 1D chains with the cations Eu^{2+} and K^+ ions spaced 4.0470(4) Å and 3.122 50(9) Å apart, respectively, within each chain. In comparison, the structure of $EuGa_2Sb_2$ is an analog with Eu^{2+} as the cation forming chains with a spacing of 4.3225(8) Å. One difference is that the anion chains of $[Ga_2Sb_2]^{2-}$ form smaller networks of tetrahedral and bridging Sb in a square-chain ladder format instead of face-sharing octahedral in the other two structures. This pseudo-Hollandite structure in $EuGa_2Sb_2$ is also structurally distinct from other pseudo-Hollandite structures such as $PbIr_4Se_8$ and $TlCr_5Se_8$ which have occupancy of non-magnetic Tl^{1+}/Pb^{2+} in the channels providing charge balance to the magnetic transition metals [32,33]. In all cases there are nonsymmorphic glide plane symmetries present that relate channel ions in adjacent channels.

B. Heat capacity

Temperature-dependent heat capacity measurements were carried out to understand the magnetic contribution of Eu and phononic contribution in the $EuGa_2Sb_2$ single crystals. Figure 2 shows the heat capacity as a function of temperature in $EuGa_2Sb_2$ from 2-225 K. The heat capacity plot showed a sharp phase transition at $T = 7.4$ K. At $T = 225$ K, the Dulong-Petit limit was observed. This limit is calculated using the $C_p = 3NR$, where N is the number of atoms and R is the ideal gas constant [34]. In $EuGa_2Sb_2$, the number of atoms is five, and the value is approximately equal to 124 J mol^{-1} K^{-1}, respectively. In order to generate the change in entropy from the magnetic order, the phonons were subtracted by modeling the high-temperature specific heat using a 2-debye phonon model and then removing that as the phonon contribution at all temperatures. The 2-debye model is

$$\frac{C_p}{T} = \frac{C_D(\theta_{D1}, s_1, T)}{T} + \frac{C_D(\theta_{D2}, s_2, T)}{T}, \quad (1)$$

$$C_D(\theta_D, T) = 9sR\left(\frac{T}{\theta_D}\right)^3 \int_0^{\theta_D/T} \frac{(\theta/T)^4 e^{\theta/T}}{[e^{\theta/T} - 1]^2} d\frac{\theta}{T}, \quad (2)$$

where θ_{D1} and θ_{D2} are the Debye temperatures, s_1 and s_2 are the oscillator strengths, and R is the molar Boltzmann constant. The model parameters from the least-squares refinement to the data for T>16 K, Fig. 3(a), are given in Table IV. The total oscillator strength $s_1 + s_2 = 5.2(2)$. This is in good agreement with the expected value of $1 + 2 + 2 = 5$, the total number of atoms per formula unit in $EuGa_2Sb_2$.

After subtracting this phonon contribution, the sample heat capacity from $T = 2$–225 K was integrated to determine the change in entropy corresponding to magnetic order in $EuGa_2Sb_2$. Figure 3(b) shows that the change in the magnetic entropy reaches a maximum of $\Delta S_{mag} \approx 16.4$ J mol^{-1} K^{-1}, close to the $R\ln(8) = 17.2$ J mol^{-1} K^{-1} expected for an

TABLE III. Anisotropic displacement parameters for $EuGa_2Sb_2$ determined by SXRD.

	U(1,1)	U(2,2)	U(3,3)	U(1,2)	U(1,3)	U(2,3)
Eu	0.00349	0.00349	0.00325	0	0.00002	0
Ga1	0.00416	0.00369	0.00444	0	0.00001	0
Ga2	0.00381	0.00367	0.00343	0	0.00001	0
Sb1	0.00278	0.00282	0.00269	0	0.00015	0
Sb2	0.00347	0.00321	0.00351	0	−0.00026	0

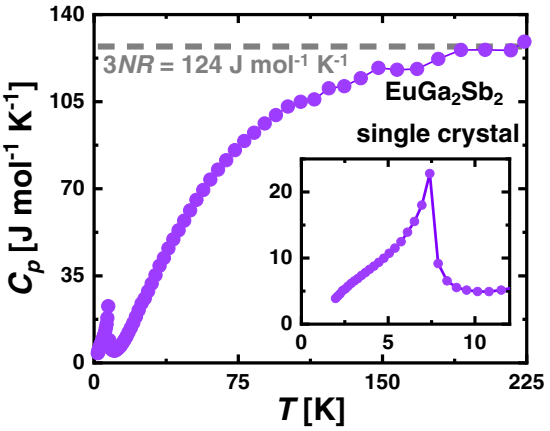

FIG. 2. Temperature-dependent heat capacity of $EuGa_2Sb_2$ single crystals at $\mu_o H = 0.1$ T from $T = 2$–225 K. The sharp transition at $T = 7$ K is attributed to the antiferromagnetic phase transition. The Dulong-Petit theoretical value of $3NR = 124\,\mathrm{J\,mol^{-1}\,K^{-1}}$ is reached around $T = 200$ K. The inset shows the magnified antiferromagnetic phase transition at $T = 7$ K.

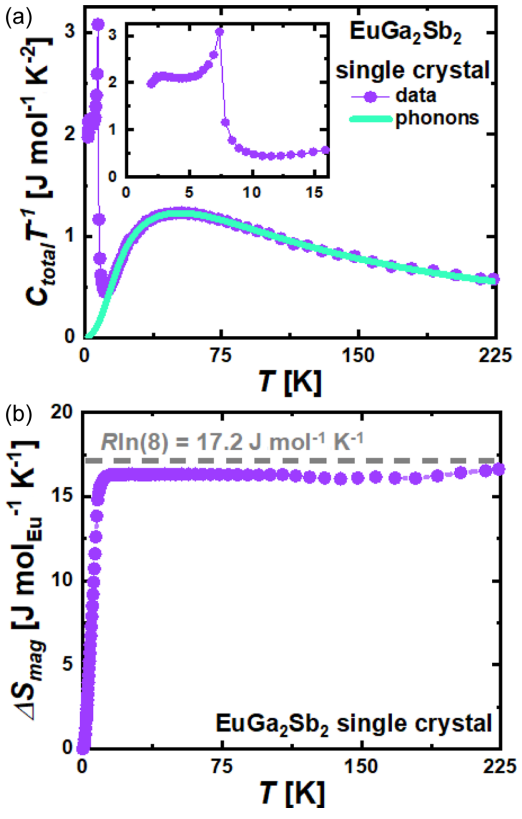

FIG. 3. (a) Heat capacity divided by temperature as a function of temperature for $EuGa_2Sb_2$ single crystals at $\mu_o H = 0.1$ T from $T = 2$–225 K. The purple is the data points, and the aqua is the phonons modeled using the 2-debye models from $T = 16$–225 K. The sharp transition at $T = 7$ K is attributed to the antiferromagnetic phase transition. (b) The change in magnetic entropy was integrated after subtracting the phonons from 2–225 K. The ΔS_{mag} is close to the $R\ln(8)$ expected for an $L = S = 7/2$ system.

TABLE IV. Fitting parameters to the Cp/T as a function of T for $EuGa_2Sb_2$ to extract the phonon contribution.

s_{D1} (Oscillator strength/formula unit)	s_{D2} (Oscillator strength/formula unit)	θ_{D1}(K)	θ_{D2}(K)
3.2(2)	2.05(9)	293(15)	121(2)

$S = 7/2$ system. The small discrepancy is attributable to the use of a linear extrapolation to capture the entropy from $T = 0$ to 2 K. The recovery of a full $R\ln(8)$ entropy is not unexpected, being seen in many divalent (Eu^{2+}) materials such as $EuMg_2Bi_2$ and $Eu_3In_2P_4$. This behavior contrasts to mixed-valent (Eu^{2+} and Eu^{3+}) compounds such as $EuZnSb_2$ and $EuIr_2In_8$ and supports our assignment of Eu^{2+} on crystal-chemical grounds [35–38]. Further, recovery of the full $R\ln(8)$ indicates minimal splitting of states due to crystal-field effects. This effect arises from the fact that $L = 0$ and that the local point symmetry of each Eu^{2+} ion is C_m: by symmetry, the ground state ${}^8S_{j=7/2}$ is allowed to split into four doublets, and the entropy from all four of these doublets must be recovered to reach $R\ln(8)$. However, the existence of these doublets may explain why the transition observed in specific heat is not a single sharp anomaly but instead has a pronounced tail extended well below the transition temperature. Third, more than 90% of the entropy is recovered below T_N. This trend indicates negligible loss of entropy above T_N, and implies a lack of low dimensional but longer range magnetic correlations. It is also important to note that in the case of Eu^{2+}, the next excited state is present at high energy such that Schottky anomalies by magnetic excited state may be safely excluded as a possibility over the measurement range [39]. Despite the structure being built of pseudo-1D chains, the physical behavior does not have a regime in which the expected 1D physics is dominant; this might be due to the large S, which is known to suppress fluctuations.

C. Magnetization

To further elucidate the magnetic properties of $EuGa_2Sb_2$, magnetization as a function of temperature and field was studied. The $M(T)$ plots in Figs. 4(a) and 4(b) show an evident antiferromagnetic phase transition at $T_N = 8.3$ K and $T_N = 7.9$ K in the parallel and perpendicular direction to the b axis, respectively. To further quantify the magnetic susceptibility results, the high-temperature, $T = 50$–300 K data were fitted to the Curie-Weiss law:

$$\chi = \frac{C}{T - \theta_{\mathrm{cw.}}} \tag{3}$$

Here C is the Curie constant, and θ_{CW} is the Weiss temperature. The fit is shown in Table V, Figs. 4(d) and 4(e), respectively. The p_{eff} extracted from the Curie constants are 8.16 and 8.15, respectively, close to the theoretical p_{eff} for Eu^{2+}, in agreement with expectations and the specific-heat results. Thus, the positive Weiss constants indicate dominant ferromagnetic interactions; in combination with the observed antiferromagnetic order, this indicates substantial antiferromagnetic and ferromagnetic interactions.

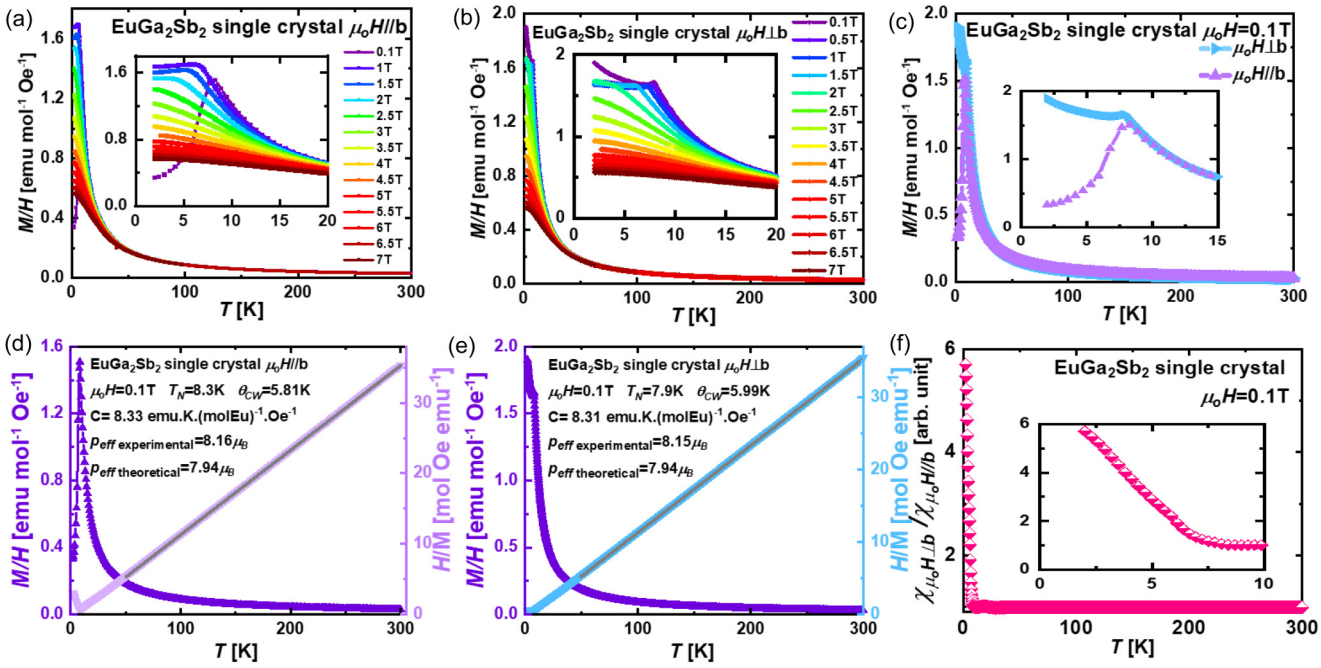

FIG. 4. (a) Magnetization as a function of temperature with $\mu_o H \parallel b$ and $\mu_o H = 0.1$–7 T and $T = 2$–300 K. The $\mu_o H = 0.1$ T data show a clear AFM transition at $T = 7$ K, with a decrease in both sharpness of the transition and the temperature of the transition as the field increases. (b) Magnetization as a function of temperature $\mu_o H \perp b$ from $\mu_o H = 0.1$–7 T and $T = 2$–300 K. The $\mu_o H = 0.1$ T data show a kink at $T = 7$ K followed by an upturn, both of which are suppressed for $\mu_o H > 0.1$ T. (c) Comparison in the magnetization as a function of temperature, $\mu_o H \perp b$ and $\mu_o H \parallel b$, at $\mu_o H = 0.1$ T over $T = 2$–300 K. (d) Curie Weiss analysis for $\mu_o H \parallel b$ from $\mu_o H = 0.1$ T in the range $T = 2$–300 K, (e) Curie Weiss analysis $\mu_o H \perp b$ from $\mu_o H = 0.1$ and $T = 2$–300 K, and (f) ratio of magnetization $\mu_o H \parallel b$ and $\mu_o H \perp b$ at $\mu_o H = 0.1$ T and $T = 2$–300 K displaying the anisotropy below T_N.

The M/H behavior is found to vary with the strength of the applied magnetic fields. The field dependence on $M(T)$ shows a decrease in the ordering temperature with increasing field at low temperatures, becoming field independent beyond $T = 40$ K in both directions. Another observation was that in $\mu_o H \perp b$, the $\mu_o H = 0.5$–2 T range had the same magnitude in magnetization at $T = 2$ K. However, the $\mu_o H \parallel b$ showed a monotonic decrease. These observations indicate the presence of anisotropy at low temperatures. Figure 4(f) shows the magnetization ratio in the parallel and perpendicular directions; above T_N, the ratio is 1, indicating no anisotropy. Below T_N, the anisotropy rises linearly, reaching a value of 6 at $T = 2$ K.

To further investigate the effect of anisotropy between the $\mu_o H \parallel b$ and $\mu_o H \perp b$ in $EuGa_2Sb_2$ single crystals, magnetization as a function of the magnetic field was studied. Figures 5(a) and 5(b) show that the effective moment reaches the theoretical saturation for Eu^{2+} in parallel and perpendicular directions along the b plane at high fields, indicative of a field-polarized state. This result further confirms the assignment of Eu valence as Eu^{2+}. Further, the shapes of the

TABLE V. Fitting parameters obtained by Curie Weiss analysis from magnetization data of $EuGa_2Sb_2$.

$EuGa_2Sb_2$	$\mu_o H \parallel b$	$\mu_o H \perp b$
Range (K)	50–300	50–300
C[emu K(mol Eu)$^{-1}$ Oe^{-1}]	8.33	8.31
θ (K)	5.81	5.99
$p_{\text{eff}}(\mu_B)$	8.16	8.15

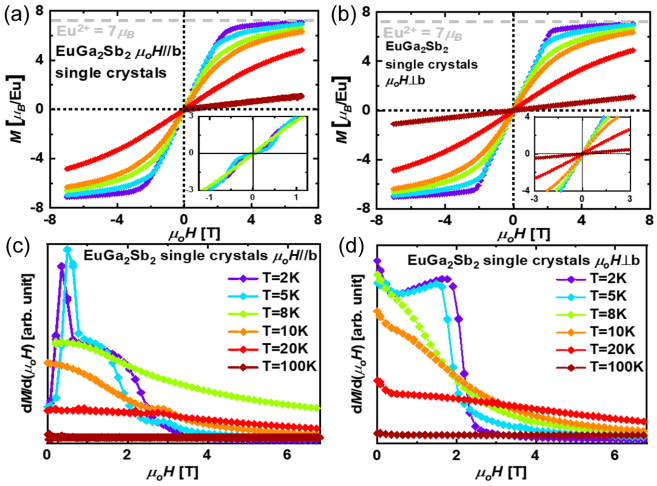

FIG. 5. (a) Magnetization as a function of magnetic field with $\mu_o H \parallel b$ from $\mu_o H = -7$ to 7 T and $T = 2$, 5, 8, 10, 20, and 100 K. (b) Magnetization as a function of magnetic field with $\mu_o H \perp b$ from $\mu_o H = -7$ to 7 T and $T = 2$, 5, 8, 10, 20, and 100 K, **(c)** derivative of magnetization over magnetic field as a function of magnetic field with $\mu_o H \parallel b$ at $T = 2$, 5, 8, 10, 20, and 100 K, and (d) derivative of magnetization over magnetic field as a function of magnetic field with $\mu_o H \perp b$ at $T = 2$, 5, 8, 10, 20, and 100 K. There is a clear metamagnetic behavior below ~0.5 T.

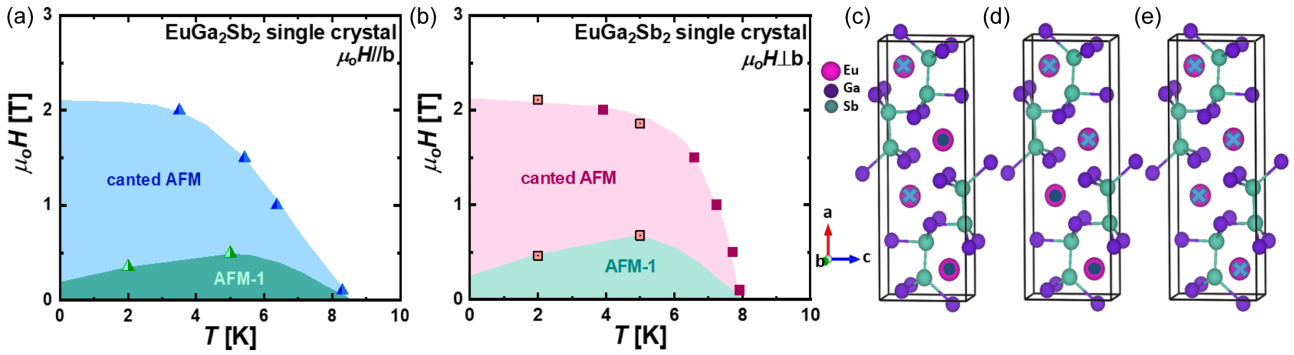

FIG. 6. (a) Magnetic phase diagram of $EuGa_2Sb_2$ with $\mu_oH \parallel b$. (b) Magnetic phase diagram of $EuGa_2Sb_2$ with $\mu_oH \perp b$. In both cases, there is an anisotropic AFM state at low fields, followed by a canted AFM state that continuously evolves to a field-polarized state. The transition from AFM-1 to canted AFM was determined from the first maximum (minimum) in the $M(H)$ derivative data for $\mu_oH \parallel b$ and $\mu_oH \perp b$, respectively. The transition from canted AFM to a field-polarized state was determined from the maximum in the $M(T)$ data. (c)–(e) Possible magnetic structures for $EuGa_2Sb_2$. In (c) and (d) the chains are ferromagnetic along the chain direction (into the page), while in (e) the chains are antiferromagnetic along the chain direction. The light blue "x" represents spin up, while the dark blue "o" represents spin down.

$M(H)$ curves are different between the two directions below T_N, consistent with the observed appearance of anisotropy.

The measurements with $\mu_oH \parallel b$ show a metamagnetic transition seen at temperatures below the ordering temperature at $\mu_oH = 0.5$ T, as seen in Fig. 5(a), inset. Metamagnetism is seen in most Co and Eu compounds because of single-ion anisotropy, but not expected here due to the isotropic nature of a $4f^7$ ($S = 7/2$) state [40,41]. Instead, we attribute this metamagnetism as a consequence of the magnetic order, which fixes the spins relative to each other, making some directions more easily polarizable than others. These behaviors can be further observed in the derivatives: Figs. 5(c) and 5(d) show the change in derivative as a function of the field from the $M(H)$ plots, which further illustrate the metamagnetic transitions in $\mu_oH \parallel b$ below T_N, while $\mu_oH \perp b$ has a monotonic trend. In general, these magnetism trends explain that the $\mu_oH \parallel b$ shows a lower induced magnetization at low applied magnetic fields. It is thus considered the hard axis (from the perspective of local spins) for ferromagnetic orders, and the easy axis in the case of antiferromagnetic order [42].

Combining these results yields the magnetic phase diagrams shown in Figs. 6(a) and 6(b). Below ~0.5 T, the system is in an antiferromagnetic state in which the applied field is not sufficient to overcome the anisotropy. Between ~0.5 and ~2 T, the spins reorient following the applied field and develop increasing (magnetic) polarization until, finally, a field-polarized ferromagnetic/paramagnetic state is reached.

From these results, we can speculate on the type of magnetic order that is present. First, the material is antiferromagnetic; this necessitates antiferromagnetic order along at least one crystal direction. Second, the positive Weiss constant suggests ferromagnetic order along at least one direction. This result leaves three possible general states, shown in Figs. 6(c), 6(d), and 6(e): ferromagnetic chains with alternating (c) or block (d) antiferromagnetic order between chains, or (e) antiferromagnetic chains with ferromagnetic order between chains. Finally, the direction of the magnetic moments is only loosely constrained: from the previous discussion in the $M(H)$ plots, it is clear that $\mu_oH \parallel b$ has smaller induced magnetization at low fields, but that can be explained either by spins that lie parallel to a with antiferromagnetic order perpendicular or by spins perpendicular to a but with ferromagnetic order parallel. Future neutron studies, challenging due to the highly absorbing nature of Eu, would be needed to discriminate between these possibilities.

IV. CONCLUSION

The structure of $EuGa_2Sb_2$ crystallizes in the space group *Pnma* (62) [23–25]. The single crystals are synthesized using the flux technique. The $EuGa_2Sb_2$ structure is characterized to be a Hollandite analog and thus having pseudo-1D chains. The change in magnetic entropy recovered reaches the theoretical limit of $R\ln(8)$ for Eu^{2+} ions, implying no frustration or fluctuations above T_N, and a small splitting in the crystal-field levels. The magnetic properties reveal that $EuGa_2Sb_2$ is anisotropic below T_N, and has a metamagnetic transition along $\mu_oH \parallel b$. The magnetic phase diagram reveals the two magnetic phases in the structure and three possibilities in the magnetic structure. Overall, our results help us gain insights into the structure and magnetism in $EuGa_2Sb_2$. For future work, neutron diffraction could further help elucidate the magnetic structure, and determine whether nonsymmorphic symmetries have any impact on the magnetic excitations that are present.

ACKNOWLEDGMENTS

This work was supported as part of the Institute for Quantum Matter and Energy Frontier Research Center, funded by the U.S. Department of Energy, Office of Science, Office of Basic Energy Sciences, under Award No. DE-SC0019331. The MPMS was funded by the National Science Foundation, Division of Materials Research, Major Research Instrumentation Program, under Award No. 1828490.

[1] H. Krebs, Acta Cryst. **9**, 95 (1956).
[2] B. Z. Eisenmann and H. Schäfer, Angew. Chem. **90**, 731 (1978).
[3] M. C. Bohm, R. Ramirez, R. Nesper, and H. G. von Schnering, Phys. Rev. B **30**, 4870 (1984).
[4] P. Sherwood and R. Hoffmann, J. Am. Chem. Soc. **112**, 2881 (1990).
[5] S. M. Kauzlarich, S. R. Brown, and G. J. Snyder, Dalton Trans. **2007**, 2099 (2007).
[6] M. Q. Arguilla, J. Katoch, K. Krymowski, N. D. Cultrara, J. S. Xu, X. X. Xi, A. Hanks, S. S. Jiang, R. D. Ross, J. R., S. Ulstrup Koch, A. Bostwick, C. Jozwiak, D. W. McComb, E. Rotenberg, J. Shan, W. Windl, R. K. Kawakami, and J. E. Goldberger, ACS Nano **10**, 9500 (2016).
[7] S.-J. Kim and M. G. Kanatzidis, Inorg. Chem. **40**, 3781 (2001).
[8] W. Liu, J. Hu, S. Zhang, M. Deng, C.-G. Han, and Y. Liu, Mater. Today Phys. **1**, 50 (2017).
[9] Y. Xu, Z. Song, Z. Wang, H. Weng, and X. Dai, Phys. Rev. Lett. **122**, 256402 (2019).
[10] T. Caillat, J.-P. Fleurial, and A. Borshchevsky, J. Phys. Chem. Solid **58**, 1119 (1997).
[11] Z. Zhu, M. Li, and J. Li, Phys. Rev. B **94**, 155121 (2016).
[12] C. Li, C. M. Wang, B. Wan, X. Wan, H.-Z. Lu, and X. C. Xie, Phys. Rev. Lett. **120**, 146602 (2018).
[13] S. K. Kushwaha, J. W. Krizan, B. E. Feldman, A. Gyenis, M. T. Randeria, J. Xiong, S. Y. Xu, N. Alidoust, I. Belopolski, T. Liang, M. Z. Hasan, N. P. Ong, A. Yazdani, and R. J. Cava, APL Mater. **3**, 041504 (2015).
[14] H. Kim and S. M. Kauzlarich, J. Solid State Chem. **178**, 1935 (2005).
[15] K. P. Devlin, J. Zhang, J. C. Fettinger, E. S. Choi, A. K. Hauble, V. Taufour, R. P. Hermann, and S. M. Kauzlarich, Inorg. Chem. **60**, 5711 8, (2021).
[16] H. B. Wu, D.-S. Ma, B. T. Fu, W. Guo, and Y. G. Yao, J. Phys. Chem. Lett. **10**, 2508 (2019).
[17] T. Berry, L. A. Pressley, W. A. Phelan, T. T. Tran, and T. M. McQueen, Chem. Mater. **32**, 5827 13, (2020).
[18] B. J. Wieder, B. Bradlyn, Z. Wang, J. Cano, Kim Y, H. S. D. Kim, A. M. Rappe, C. L. Kane, and B. A. Bernevig, Science **361**, 246 (2018).
[19] B. Bradlyn, J. Cano, Z. Wang, M. G. Vergniory, C. Felser, R. J. Cava, and B. A. Bernevig, Science **353**, aaf5037 (2016).
[20] S. Lei, V. Duppel, M. Lippmann, J. Nuss, B. V. Lotsch, and L. M. Schoop, Adv. Quantum Technol. **2**, 1900045 (2019).
[21] L. M. Schoop, A. Topp, J. Lippmann, F. Orlandi, L. Müchler, M. G. Vergniory, Y. Sun, A. W. Rost, V. Duppel, M. Krivenkov, S. Sheoran, P. Manuel, A. Varykhalov, B. Yan, R. K. Kremer, C. R. Ast, and B. V. Lotsch, Sci. Adv. **4**, eaar2317 (2018).
[22] M. M. Hosen, G. Dhakal, K. Dimitri, P. Maldonado, A. Aperis, F. Kabir, C. Sims, P. Riseborough, P. M. Oppeneer, D. Kaczorowski *et al.*, Sci. Rep. **8**, 13283 (2018).
[23] S. Chanakian, R. Weber, U. Aydemir, A. Ormeci, J. P. Fleurial, S. Bux, and J. G. Snyder, J. Elec. Mater. **46**, 4798 8, (2017).
[24] I. Schellenberg, M. Eul, and R. Pöttgen, Monatsh. Chem. **142**, 875 (2011).
[25] N. Singh, R. Pöttgen, and U. Schwingenschlögl, J. Appl. Phys. **112**, 103714 (2012).
[26] P. C. Canfield, T. Kong, U. S. Kaluarachchi, and N. H. Jo, Philos. Mag. **96**, 84 (2016).
[27] L. Krause, R. Herbst-Irmer, G. M. Sheldrick, and D. Stalke, J. Appl. Cryst. **48**, 3 (2015).
[28] G. M. Sheldrick, Acta Cryst. **64**, 112 (2008).
[29] G. M. Sheldrick, Acta Cryst. **A71**, 3 (2015).
[30] R. P. Guertina, J. Appl. Phys. **103**, 07B705 (2008).
[31] R. D. McAuliffe, C. A. Miller, X. Zhang, B. S. Hulbert, A. Huq, C. Cruz, A. Schleife, and D. P. Shoemaker, Inorg. Chem. **56**, 2914 (2017).
[32] B. A. Trump and T. M. McQueen, J. Solid State Chem. **242**, 112 (2016).
[33] K. Klepp and H. Boller, J. Solid State Chem. **48**, 388 (1983).
[34] H. A. Bent, J. Chem. Educ. **57**, 395 (1980).
[35] S. Pakhira, M. A. Tanatar, and D. C. Johnston, Phys. Rev. B **101**, 214407 (2020).
[36] J. Jiang, M. M. Olmstead, S. M. Kauzlarich, H. O. Lee, P. Klavins, and Z. Fisk, Z. Inorg. Chem. **44**, 5322 (2005).
[37] A. Wang, S. Baranets, Y. Liu, X. Tong, E. Stavitski, J. Zhang, Y. Chai, W.-G. Yin, S. Bobev, and C. Petrovic, Phys. Rev. Res. **2**, 033462 (2020).
[38] N. P. Calta, S. L. Budko, A. P. Rodriguez, F. Han, D. Y. Chung, and M. G. Kanatzidis, Inorg. Chem. **55**, 3128 (2016).
[39] P. Fulde and M. Loewenhaupt, Adv. Phys. **34**, 589 (1985).
[40] H. K. Vivanco, B. A. Trump, C. M. Brown, and T. M. McQueen, Phys. Rev. B **102**, 224411 (2020).
[41] L. Holmes and M. Schieber, J. Appl. Phys. **37**, 968 (1966).
[42] K. Yosida, *Theory of Magnetism* (Springer, Berlin, 1991).